Hydration of Sulfo and Methyl Groups in Dimethyl Sulfoxide Is Accompanied by the Formation of Red-Shifted Hydrogen Bonds and Improper Blue-Shifted Hydrogen Bonds: An ab Initio Quantum Chemical Study

Eva Mrázková[†] and Pavel Hobza*

J. Heyrovský Institute of Physical Chemistry, Academy of Sciences of the Czech Republic and Center for Complex Molecular Systems and Biomolecules, Dolejškova 3, 182 23 Prague 8, Czech Republic

Received: September 3, 2002; In Final Form: November 15, 2002

In this study, the hydration of dimethyl sulfoxide was investigated by means of molecular dynamics (MD) simulations and quantum chemical correlated ab initio calculations. MD simulations show the hydration sites when the systems are exposed to 1, 3, 6, 16, and 32 water molecules. Various DMSO···$(H_2O)_n$ ($n = 1-3$) complexes where waters hydrate sulfo and methyl groups were then reoptimized at the ab initio level. The hydration of DMSO leads to an elongation of the S═O bond and a contraction of methyl C−H bonds. Whereas the elongation of the S═O bond is accompanied by a red shift of the respective stretch frequency, the contraction of the C−H bonds gives a blue shift to the C−H stretch frequencies. The former effect is easily explained by the transfer of electron density to the antibonding orbitals of the S═O bond, yielding its weakening. Various mechanisms leading to the contraction of the methyl CH bonds were suggested. They were based on secondary geometry changes originating from the significant elongation of the S═O bond and also on the changes of the electron density in DMSO upon complexation, resulting in a rehybridization of the CH bonds. The influence of the electrostatic field of hydrating waters was also considered. Predicted frequency shifts fully agree with the observed data. Also, the observed blue shift increase occurring as a consequence of progressive hydration was interpreted theoretically, and the mechanisms of this phenomenon are suggested.

I. Introduction

The hydration of alkyl groups of various water-soluble systems surprisingly is accompanied by a C−H stretch frequency increase instead of the expected frequency decrease. This was observed experimentally for dimethyl sulfoxide (DMSO), hexamethylphosphoricacidtriamide, acetonitrile, acetone, THF, DMF and HMPT,[1] *n*-propylamine, piperidine, morpholine and 1,4-dioxane,[2] ethanol,[3] and phosphocholine.[4]

The hydration of DMSO, yielding a red shift of the S═O stretch frequency and a blue shift of the C−H stretch frequencies, was studied using IR and NMR spectroscopy.[5] How can it be explained that the hydration of the S═O group in DMSO gives a red shift of its stretch frequency whereas the hydration of the CH_3 group gives a blue shift of its stretch frequencies? Is the standard hydrogen (H)-bond formed in both cases? Following the definition of a hydrogen bond,[6] we must answer no. The H-bond is, according to ref 6, characterized by the elongation of the X−H bond, a decrease of its stretch frequency, and an increase of the intensity of the respective spectral band. These features are called fingerprints of H bonding, and no exceptions have been mentioned in ref 6 (the book appeared in 1997). However, in going carefully through the literature, one finds exceptions. In 1980, Sandorfy et al.,[7] when measuring the association of fluoroparaffines containing the $-CHF_2$ group with various proton acceptors, reported the shift of the C−H stretch frequency to higher values. Further experimental evidence of the blue shift of the C−H stretch frequency appeared in 1989[8] and 1997.[9] The first systematic investigation of the blue shift of the C−H stretch frequency was a theoretical study of the interaction of benzene with various C−H proton donors.[10] Because the most important features of the studied C−H···π interactions (contraction of the C−H bond, blue shift of the C−H stretch frequency) were opposite to these in the H bonds, we called[11] this specific bonding type an "improper, blue-shifting" hydrogen bond.

Until now, various types of improper blue-shifting hydrogen bonds containing the X−H proton donor and various proton acceptors were detected experimentally in the gas or liquid phase or were discovered theoretically.[12−25]

The mechanism of H-bonding can be interpreted using electrostatic and charge-transfer models. The realistic picture of H bonding is, however, based on a combination of both models. Electrostatic and charge-transfer approaches complement each other, and only in borderline cases does one approach becomes dominant. The classical picture of H-bonding is based on the interaction of lone-pair orbitals of the proton acceptor with the σ^* antibonding orbitals of the proton donor. A very similar picture is obtained using natural bond orbital (NBO) analysis. Weinhold et al.[26] demonstrated that the charge transfer from lone electron pairs of an electron donor is directed to the X−H σ^* antibonding orbitals of the proton donor. The increase of electron density in antibonding orbitals weakens the X−H bond, which leads to its elongation and concomitant lowering of the X−H stretch frequency. Performing the same type of analysis for complexes with improper blue-shifting hydrogen bonds, we have shown[11] that charge transfer (again from lone pairs of an electron donor) is now directed to the remote (nonparticipating) parts of the electron acceptor, which causes

* Corresponding author. E-mail: hobza@indy.jh-inst.cas.cz.

[†] Undergraduate student in the Department of Physical and Macromolecular Chemistry, Faculty of Sciences, Charles University, Prague, Czech Republic.

10.1021/jp026895e CCC: $25.00
Published on Web 01/24/2003

geometrical changes in that part of the electron acceptor. This primary effect is accompanied by a secondary effect of the structural reorganization of the electron acceptor, leading to the contraction of the X−H bond and a blue shift of the X−H stretch frequency.

Let us point out here that some features of improper H-bonding may be interpreted by the electrostatic model, specifically by optimizing the structure of the proton donor in the electrostatic field of the proton acceptor (for further details, see ref 20). However, a full description of improper H-bonding (as well as H-bonding; see above) can be obtained only through a combination of both models.[23]

In the present work, we report a theoretical investigation (using molecular dynamics (MD) simulations and ab initio quantum chemical calculations) of the hydration of DMSO with the aim of finding the nature of binding at sulfo and methyl heads and interpreting the experimental findings of the linear increase of the C−H blue shifts with progressive hydration.

II. Strategy of Calculations

The first and most essential question is what the hydration shell of DMSO looks like. Are the waters predominantly hydrating the S═O group or the nonpolar CH_3 groups as well? This problem cannot be solved by ab initio calculations but only by MD simulations. The hydration of DMSO was recently studied by MD simulations,[27] but no evidence was reported on the simultaneous hydration of both heads. It is thus necessary to analyze the MD trajectories with the aim of extracting information on the hydration of methyl groups. Microhydrated structures of DMSO will in the second step be reoptimized at the ab initio level, and their stabilization energies and vibrational frequencies will be also determined. The hydration of DMSO will be also studied by a continuous solvation model.

The NBO analysis, which correlates well with changes in bond lengths, provides characteristics that are closely connected to basic chemical concepts. The NBO analysis will be used to generate information on the changes of electron densities in proton donors and proton acceptors as well as in the bonding and antibonding space. We are aware of shortcomings of the NBO analysis (the method overestimates the charge transfer, for example), but the splitting of changes of electron density between the bonding and antibonding space is essential for estimating the strengthening or weakening of a bond upon complexation. The changes in total electron density are certainly free of any model assumptions, but they do not tell us anything about the energetics of a bond (see, for example, ref 28). In other words, an increase or decrease of the total electron density does not give any information about the strengthening or weakening of a bond. Such information can be obtained only from an analysis of electron density changes in bonding and nonbonding space. Electron densities transferred between subsystems are small, but these values are chemically significant. Very roughly, 0.001e of charge transfer corresponds to 1 kcal/mol of stabilization energy.

The effect of the electrostatic field of water molecules on the geometrical properties of the DMSO molecule will be studied as well.

III. Calculations

III.1. MD Simulations. MD simulations were carried out in the microcanonical *NVE* ensemble (*N*, *V*, and *E* represent the number of particles, volume, and energy, respectively) using quick temperature scaling; the temperature was held at about 300 K. The time step in all simulations was 0.2 fs, and the SHAKE algorithm for the handling of very quick O−H vibrations was not used. The total duration of the simulations was 1 ps, which is long enough for a proper sampling of the configuration space. All calculations were performed using the AMBER 6.0 code with the TIP3P potential for water molecules.

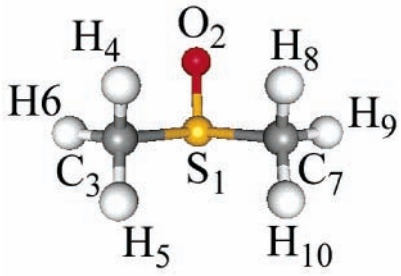

S_1	0.371
O_2	-0.515
C_3	-0.446
H_4	0.190
H_5	0.149
H_6	0.188
C_7	-0.507
H_8	0.201
H_9	0.204
H_{10}	0.169

Figure 1. Structure of optimized DMSO (RI-MP2/TZVPP level) with atomic charges according to the Merz−Kollman scheme.

III.2. Quantum Chemical ab Initio Calculations. Structures of DMSO (Figure 1) as well of DMSO···$(H_2O)_n$ ($n = 1-3$) complexes (Figures 2−4) were optimized at the RI-MP2/TZVPP [5s3p2d1f/3s2p1d] and MP2/6-31G** levels of theory. The former level yields accurate geometries of isolated systems as well as complexes. We have proved this recently by calculating the rotational constants of canonical cytosine[29] and the phenol dimer.[30] The RI-MP2/TZVPP results mentioned above were in both cases close to the experimental values. This was also an argument as to why we did not use the theoretically justified but computationally tedious counterpoise-corrected geometry optimization. Stabilization energies were determined for optimized structures. Basis set extension effects were eliminated using the Boys−Bernardi function counterpoise method, [31] and the deformation energy was also evaluated.

A harmonic vibrational analysis was performed using numerical (RI-MP2) and analytical (MP2) procedures. The RI-MP2 and MP2 calculations were performed using Turbomole[32] and Gaussian 98[33] codes, respectively. The NBO analysis implemented in Gaussian 98 was evaluated using the MP2 geometries and B3LYP electron densities. The reason is that the NBO treatment requires well-defined one-electron densities.

The electrostatic calculations were performed in the field created by point charges evaluated by using the Merz−Singh−Kollman scheme as implemented in the Gaussian 98 code. Optimization was performed with respect to either selected coordinates only or all degrees of freedom.

The continuous solvent calculations were made using the COSMO[34] procedure (DFT/B3LYP/6-31G** level) as implemented in the Gaussian 98 code.

IV. Results and Discussion

IV.1. Structure of Molecular Clusters Determined by the MD Simulations. The DMSO···H_2O complex was studied first.

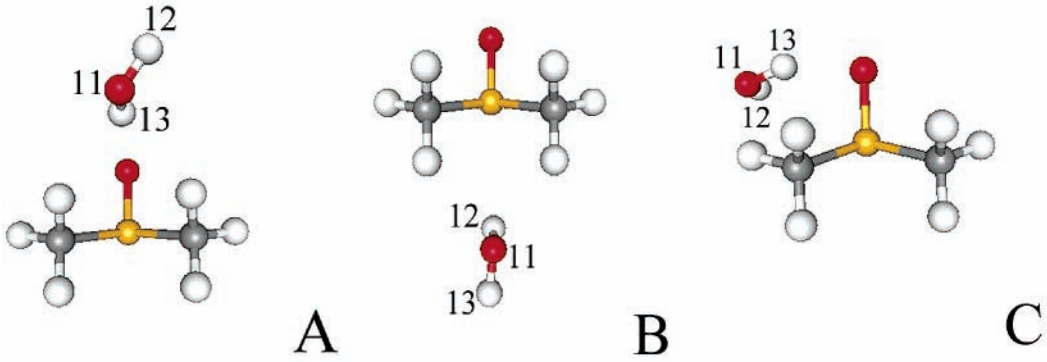

Figure 2. Structures of optimized clusters of DMSO···H_2O.

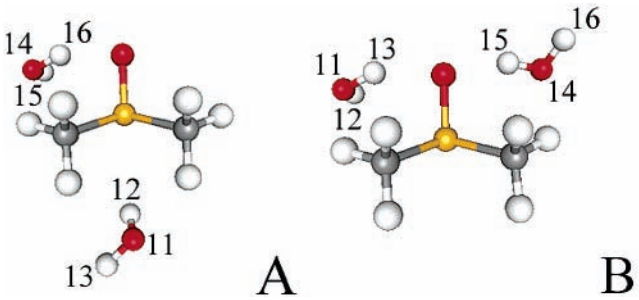

Figure 3. Structures of optimized clusters of DMSO···$(H_2O)_2$.

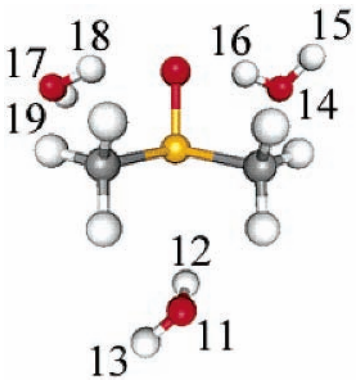

Figure 4. Structure of the optimized cluster of DMSO···$(H_2O)_3$.

The histograms showing the distribution of S−O_{water} distances (Figure 5), (S−O)−O_{water} angles, and (C−S−O)−O_{water} dihedrals (not presented) are consistent with the existence of only one structure where water hydrates the oxygen of DMSO. The red (dashed) line in Figure 5 exhibits a sharp peak at about 4.6 Å, which supports the existence of only one complex structure. Other structures were not apparent during the simulations. In the case of DMSO···$(H_2O)_3$, the simulation is different, and a histogram showing the S−O_{water} blue (dotted) line in Figure 5 exhibits the broader (double) peak between 4.7 and 5.5 Å. The first peak corresponds to the interaction of two waters with the oxygen of DMSO (analogous to the previous case) whereas the second peak gives evidence that the third water did not directly hydrate the DMSO but interacted with two other waters. Extending the hydration shell to six waters, we obtained basically the same picture (i.e., waters preferentially made the hydration shell around the polar S═O group). A change in the hydration picture occurred for DMSO···$(H_2O)_{16}$ and DMSO···$(H_2O)_{32}$ complexes, where waters interact directly not only with the S═O group but also with both methyls. The histogram showing the distribution of S−O_{water} distances for the last complex, shown by the green (solid) line in Figure 5, exhibits a symmetrical shape with a maximum at about 8 Å, which provides evidence concerning the existence of the hydration shell where waters interact with all parts of DMSO (i.e., with the S═O group as well as with both methyl groups).

IV.2. Geometry and Properties of DMSO and DMSO···Water Complexes Determined by ab Initio Calculations. DMSO. The optimized structure and its atomic charges are presented in Figure 1, and the respective bond lengths are given in Table 1.

DMSO···H_2O. MD simulations show that water preferentially hydrates the S═O group, but for higher hydration numbers, the methyl groups are hydrated also. We therefore selected three model structures corresponding to the hydration of S═O and methyl groups or to the simultaneous hydration of both groups. The optimized structures of these three structures are illustrated in Figure 2, and their stabilization energies and geometrical characteristics are given in Table 2.

Following the expectation, structures A and C, where water interacts with the S═O group, are more stable than structure B, and also the RI-MP2/TZVPP stabilization energies are larger than those of the MP2/6-31G** level. The S═O bond is elongated upon complexation in structures A and C, and these changes are rather large; the MP2/6-31G** calculations give systematically larger elongations. A considerably smaller change of the S═O bond as a consequence of hydration appeared in structure B, and more reliable RI-MP2/TZVPP calculations yield only a negligible change. Evidently, in structures A and C, an H bond between an oxygen atom in the S═O group and the hydrogen in water is formed, and the S═O and O−H bonds are elongated. Table 2 further shows that the S−C bonds in all structures are contracted and that these contractions are about 1 order of magnitude smaller in absolute value than the changes in the S═O bond. Changes in the C−H bonds are the smallest (cf. Table 2) and are similar for all structures. Considering the more reliable RI-MP2 results, we find that the C−H bonds are mainly contracted upon complexation with water, and the largest contraction was found for the C_3−H_4 (structures A and B) and C_7−H_9 (structure C) bonds. From Figure 2, it is evident that these bonds are exposed to water.

Summarizing the bond length changes, we found the largest changes for the S═O bond (with the exception of structure B), followed by decreases of both C−S bond lengths by 1 order of magnitude and changes of the C−H bonds that are again smaller by 1 order of magnitude. Although the changes of the S═O and C−S bonds are similar for all structures, the C−H bond changes are different; some of these bonds are contracted, and others are elongated.

Table 3 shows the absolute values of selected vibrational frequencies of DMSO as well as their changes upon hydration. The relative values of C−H, S═O, and O−H stretch vibrations basically agree with the presented geometrical changes. The S═

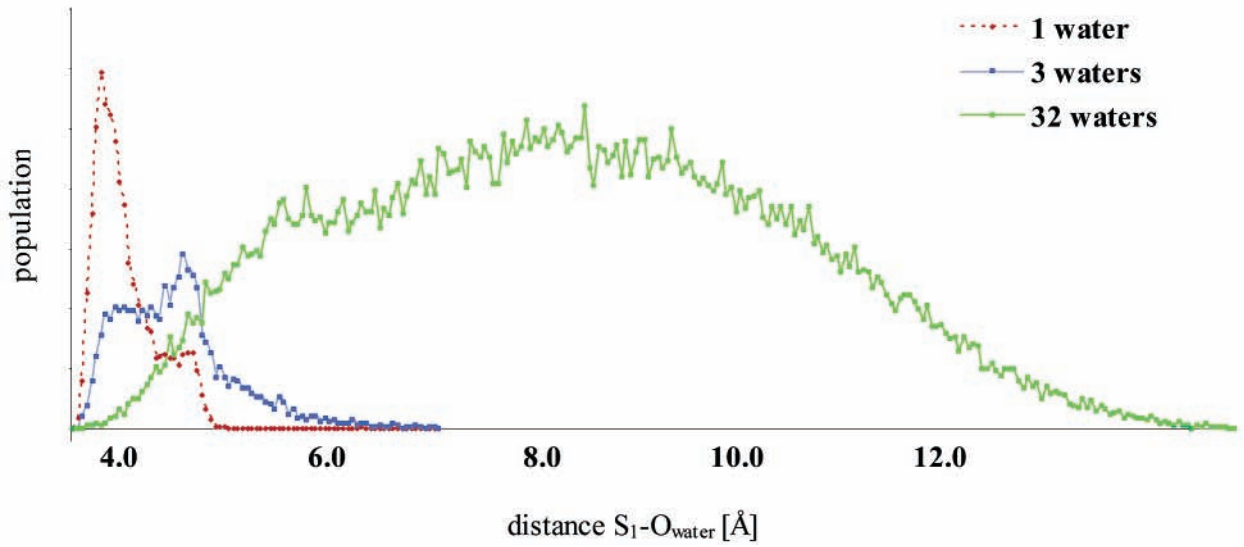

Figure 5. Histogram showing the population of S−O_{water} distances for DMSO···$(H_2O)_n$, $n = 1, 3, 32$.

TABLE 1: Bond Lengths (Å) of Isolated DMSO[a]

	RI-MP2/TZVPP	MP2/6-31G**
S_1-O_2	1.5005	1.5110
S_1-C_3	1.8031	1.8075
C_3-H_4	1.0881	1.0887
C_3-H_5	1.0881	1.0887
C_3-H_6	1.0863	1.0869
S_1-C_7	1.8038	1.8078
C_7-H_8	1.0881	1.0887
C_7-H_9	1.0863	1.0869
C_7-H_{10}	1.0881	1.0887

[a] See Figure 1.

O and O−H stretch vibrations in structures A and C are red-shifted. The changes of these vibrations in structure B are much smaller. The RI-MP2 and the MP2 values agree well. Practically all C−H stretches are blue-shifted upon complexation, and again both theoretical levels yield similar values. The largest shifts of the C−H stretch frequencies were found for structure B, where both methyl groups interact with water, but smaller shifts were also detected in two other structures where direct contact between methyl groups and water is missing.

The results of the NBO analysis are in accord with the data presented. Table 6 shows the most significant changes in electron density (ED) for different structures of DMSO···$(H_2O)_n$. In dimer A, the DMSO acts as an electron donor (0.031e), and water, as an electron acceptor. The significant changes in ED are connected with the decrease in ED in the σ^* antibonding orbitals of both S−C bonds, which causes a strengthening of these bonds. A large increase of ED was detected in the $O_{11}-H_{12}$ σ^* antibonding orbital, which gives a weakening and elongation of the water O−H bond and a concomitant red shift of the O−H stretch frequencies. ED also increased in the S═O and C_3-H_4 σ^* antibonding orbitals, which is what gives the elongation of these bonds. In this case, the standard S═O···H−O H-bond is formed, S═O as well as O−H bonds are elongated, and their stretch frequencies are red-shifted (cf. Table 3). In dimer C, DMSO again acts as an electron donor (0.028e), and water, as an electron acceptor. The largest changes of ED are again connected with the ED decrease in the σ^* antibonding orbitals of the S−C bonds and the ED increase in the $O_{11}-H_{13}$ σ^* antibonding orbital of water. Similarly, as in the previous case, the ED also increased in the S═O σ^* antibonding orbital, which is what gives the elongation of this bond. Putting all of these effects together, we obtain a weakening of the S═O and O−H bonds followed by their elongation and red shifts of their stretch frequencies (cf. Table 3). This means that the standard S═O···H−O H-bond is again formed. The NBO analysis does not support the contraction of the C−H bonds, and in the case of dimer A, we obtained an ED increase in the C_3-H_4 antibonding orbital, which results in the elongation

TABLE 2: Changes in Bond Lengths (Å) of DMSO and Water upon Complexation and Interaction Energies (ΔE, kcal/mol) for DMSO···(H_2O) Clusters[a]

	dimer A		dimer B		dimer C	
	RI-MP2/TZVPP	MP2/631G**	RI-MP2/TZVPP	MP2/6-31G**	RI-MP2/TZVPP	MP2/6-31G**
ΔE	−9.27	−8.27	−3.56	−2.83	−7.77	−6.59
S_1-O_2	0.0138	0.0162	−0.0001	0.0015	0.0129	0.0149
S_1-C_3	−0.0029	−0.0039	−0.0028	−0.0027	−0.0053	−0.0059
C_3-H_4	−0.0002	−0.0007	−0.0002	−0.0000	−0.0004	−0.0004
C_3-H_5	−0.0000	−0.0002	−0.0000	−0.0014	−0.0001	−0.0002
C_3-H_6	0.0001	0.0001	0.0001	0.0003	−0.0001	−0.0002
S_1-C_7	−0.0036	−0.0043	−0.0036	−0.0029	−0.0060	−0.0072
C_7-H_8	−0.0001	−0.0006	−0.0001	−0.0000	0.0000	−0.0000
C_7-H_9	0.0000	0.0000	0.0001	0.0003	0.0004	−0.0003
C_7-H_{10}	−0.0001	0.0000	−0.0001	−0.0015	−0.0001	0.0000
$H_{12}-O_{11}$	0.0181	0.0159	0.0007	0.0007	−0.0005	0.0002
$H_{13}-O_{11}$	−0.0005	−0.0000	0.0028	0.0017	0.0135	0.0113

[a] See Figure 2.

TABLE 3: Vibrational Frequencies and Their Changes in DMSO and DMSO···$(H_2O)_n$ Complexes Evaluated at the (a) RI-MP2/TZVPP and (b) MP2/6-31G Levels[a]**

		isolated system		dimer A		dimer B		dimer C		trimer A		trimer B		tetramer	
		a	b	a	b	a	b	a	b	a	b	a	b	a	b
	antisym	3212	3261	1	3	6	9	3	8	8	16	6	12	12	19
	antisym	3211	3260	1	3	4	8	2	4	8	12	5	8	11	18
C−H	antisym	3202	3251	4	6	2	2	3	3	6	8	4	3	7	13
stretch	antisym	3199	3248	3	5	4	4	1	1	6	10	5	4	10	12
	antisym	3085	3132	1	3	2	4	3	2	6	7	2	2	6	9
	sym	3081	3131	0	1	2	4	−1	0	2	7	2	1	4	8
S═O	bond stretch	1091	1146	−37	−36	2	1	−39	−43	−40	−40	−71	−71	−77	−148
water	antisym	3978	4030	−315	−253	−34	−18	−222	−159	−28	−23	−191	−145	−20	−22
O_{11}	sym	3856	3892	−49	−61	−28	−18	−47	−58	−26	−20	−45	−58	−19	−19
water	antisym	3978	4030							−237	−181	−205	−159	−205	−164
O_{14}	sym	3856	3892							−45	−60	−43	−56	−46	−59
water	antisym	3978	4030											−222	−179
O_{17}	sym	3856	3892											−41	−60

[a] A positive number indicates a blue shift and a negative number, a red shift.

TABLE 4: Changes in Bond Lengths (Å) of DMSO and Water upon Complexation and Interaction Energies (ΔE, kcal/mol) for DMSO···$(H_2O)_2$ Clusters[a]

	trimer A		trimer B	
	RI-MP2/TZVPP	MP2/6-31G**	RI-MP2/TZVPP	MP2/6-31G**
ΔE	−10.43	−9.17	−14.56	−13.13
S_1-O_2	0.0138	0.0171	0.0256	0.0302
S_1-C_3	−0.0083	−0.0089	−0.0094	−0.0103
C_3-H_4	−0.0004	−0.0005	−0.0004	−0.0004
C_3-H_5	−0.0009	−0.0015	−0.0002	−0.0003
C_3-H_6	−0.0000	0.0000	0.0001	−0.0002
S_1-C_7	−0.0083	−0.0090	−0.0102	−0.0114
C_7-H_8	−0.0000	−0.0002	−0.0003	−0.0004
C_7-H_9	0.0004	−0.0001	0.0003	−0.0006
C_7-H_{10}	−0.0009	−0.0019	−0.0003	−0.0001
$H_{12}-O_{11}$	0.0009	0.0012	−0.0006	0.0004
$H_{13}-O_{11}$	0.0024	0.0021	0.0124	0.0106
$H_{15}-O_{14}$	−0.00074	0.00019	0.01226	0.01117
$H_{16}-O_{14}$	0.01437	0.01252	−0.00069	0.00019

[a] See Figure 3.

of this bond. This unambiguously means that contractions in C−H bond lengths and increases in C−H stretch frequencies were not due to direct ED transfer but rather to some secondary effect.

In the case of dimer B, the ED transfer (EDT) (0.0047e) is about 1 order of magnitude smaller than in dimers A and C. All of the changes of ED are smaller than in previous complexes and are thus not presented in Table 6. Evidently, the contraction of C−H bonds and blue shifts of their stretching vibrations in this dimer are due to other mechanisms (discussed later).

DMSO···$(H_2O)_2$. Optimized structures of both trimers are shown in Figure 3, and their characteristics are brought together in Table 4. It must be mentioned here that the investigated complexes do not correspond to the most stable structures of the DMSO···$(H_2O)_2$ complexes, where a direct water−water contact should be present. From the performed MD simulations (see above), we know, however, that in the case of higher hydrates of DMSO (16 and 32 water molecules) waters interacts with the S═O group as well as with the methyl groups. The trimer structures A and B thus represent only model interaction types that occur if higher numbers of water molecules are present. Structure A, where waters hydrate the S═O as well as the methyl groups, is less stable than structure B where both waters hydrates the S═O group. The RI-MP2 stabilization energy is again larger than the MP2 energy. Analyzing the geometrical changes in trimer structure A upon complexation, we found that the S═O and $O_{14}-H_{16}$ bonds are elongated similarly as in dimers A and C whereas the elongation of the S═O bond in trimer B is approximately twice as large. Also, both O−H bonds of two waters interacting with the S═O bond ($O_{11}-H_{13}$ and $O_{14}-H_{16}$) are elongated, and this elongation is similar to that occurring in dimers A and C. Both S−C bonds in both trimers are contracted, and surprisingly, these contractions are larger for trimer B. The contraction of the S−C bonds in trimers is much larger than in dimers and is comparable (in absolute value) to the elongation of the S═O bond. Investigating the geometrical changes of the C−H bonds, we found that practically all C−H bonds in both trimer structures are contracted, the RI-MP2 and MP2 values being roughly comparable. The largest contraction was observed for the C_3-H_5 and C_7-H_{10} bonds, which are exposed directly to water O_{11}. A similar situation was also discovered in dimer structure B, but the contraction of these two bonds was considerably smaller. Evidently, the cooperative effect of the second water (O_{14}) that hydrates the S═O group is responsible for magnifying the geometrical changes of all CH bonds.

Vibrational analysis (cf. Table 3), performed at the RI-MP2 and MP2 levels, tells us that the shift of the S═O stretch vibrational frequency in trimer B, where both waters hydrate the S═O group, is about twice as large and that it is a direct consequence of dihydration. In trimer A, where one water hydrates the methyl groups and the second water interacts with the S═O group, the vibrational stretch frequency changes very little. Blue shifts of C−H stretch vibrational frequencies in trimer A are larger than those in trimer B, which supports the role of direct hydration. However, the fact that the C−H stretch vibrational frequency shifts in trimer B (where only one water is in contact with the methyl groups) are larger than those in all of the dimers supports a different origin of the C−H blue shifts.

The NBO analysis performed for the DMSO···$(H_2O)_2$ trimer (structure A) shows that both mechanisms suggested for dimers B and C took place. One water acts as a proton acceptor (−0.02477e) whereas the second one acts as a proton donor (0.00716e). The largest change of ED (Table 6) corresponds to an increase of ED in the $O_{14}-H_{16}$ σ^* antibonding orbital, leading to a significant elongation of this bond (cf. Table 2) and a red shift of the respective stretch vibration (cf. Table 3). The

TABLE 5: Changes in Bond Lengths (Å) of DMSO and Water upon Complexation and Interaction Energies (ΔE, kcal/mol) for DMSO···$(H_2O)_3$ Clusters[a]

	tetramer	
	RI-MP2/TZVPP	MP2/6-31G**
ΔE	−17.75	−16.05
S_1-O_2	0.0278	0.0335
S_1-C_3	−0.0117	−0.0126
C_3-H_4	−0.0005	−0.0004
C_3-H_5	−0.0011	−0.0018
C_3-H_6	0.0003	−0.0004
S_1-C_7	−0.0125	−0.0135
C_7-H_8	−0.0004	−0.0006
C_7-H_9	0.0004	−0.0004
C_7-H_{10}	−0.0012	−0.0022
$H_{12}-O_{11}$	0.0008	0.0013
$H_{13}-O_{11}$	0.0019	0.0021
$H_{15}-O_{14}$	−0.0006	0.0003
$H_{16}-O_{14}$	0.0132	0.0117
$H_{18}-O_{17}$	0.0130	0.0121
$H_{19}-O_{17}$	−0.0009	0.0003

[a] See Figure 4.

situation in trimer B is similar, and Table 6 shows strong similarities with trimer A. Both water molecules in this complex act as electron acceptors. The largest changes of ED occur at the waters' OH σ^* antibonding orbitals, leading to the elongation of these bonds and red shifts of their stretch vibrational frequencies. Both structures are characteristic, with the decrease of ED in the S−C σ^* antibonding orbitals leading to the bond contraction and the increase of ED in the S═O antibonding orbitals leading to an elongation of this bond. Evidently, two standard S═O···H−O H-bonds are formed. The contraction of C−H bonds and the blue shifts of their stretch frequencies in both trimers are again not supported by any suitable changes of ED (i.e., an increase of ED in the σ bonding orbitals or a decrease of ED in the σ^* antibonding orbitals) and can thus be explained only by the secondary effects or by electrostatic effects (discussed later).

DMSO···$(H_2O)_3$. The largest cluster was investigated again at both theoretical levels; its optimized structure is depicted in Figure 4, and the stabilization energy and the geometrical changes due to complexation are summarized in Table 5. Figure 4 illustrates that two waters hydrate the S═O group whereas the third one is placed between both methyl groups. The elongation of the S═O bond in the tetramer is slightly larger than that in trimer B, which demonstrates that the third water (O_{11}) also affects the hydration pattern at the S═O group, though to a smaller extent than the two previous waters. The same is roughly true regarding the contraction of both C−S bonds. The largest contraction among all C−H bonds was found (similar to that of trimer A) for C_3-H_5 and C_7-H_{10} bonds, and in the present tetramer, it is about 20% larger. The geometrical changes of S═O and S−C bonds are comparable (in absolute value) and are about 1 order of magnitude larger than those of the C−H bonds.

Vibrational analysis (Table 3) shows that the third water placed between the two methyl groups enhanced the blue shifts of all of the C−H stretch frequencies whereas the red shift of the S═O stretch frequency increased slightly. The average blue shift of the C−H stretch frequencies in dimers A, B, and C (2, 3, and 2 cm^{-1}, respectively) increases to 6 and 4 cm^{-1} in trimers A and B, respectively, and to 10 cm^{-1} in the tetramer (RI-MP2 calculations). Following the RI-MP2 calculations, the red shift of the S═O stretch frequency increases from 39 cm^{-1} in dimer C to 71 cm^{-1} in trimer B to 77 cm^{-1} in the tetramer. Evidently, the red shift of the S═O stretch is close to saturation, and the most important increase was connected with the second water. However, blue shifts of the CH stretch frequency increased almost linearly with hydration number and are probably still far from the saturation point.

TABLE 6: Electron Density Transfer (EDT, [e]) and Selected Differences (larger than 0.0015e) between Electron Density (ED) Values in Complexes and Isolated Systems Calculated at the B3LYP/6-31G Level**

DMSO···$(H_2O)_n$	$n=1$	$n=2$		$n=3$
structure	A	C	A	B	
σ S_1-O_2				−0.00170	−0.00163
σ^* S_1-O_2	0.00411	0.00313	0.00653	0.00595	0.00990
σ^* S_1-C_3	−0.01750	−0.01976	−0.02160	−0.03277	−0.03407
σ^* C_3-H_4	0.00583				
σ^* C_3-H_5			0.00153		0.00197
σ^* C_3-H_6				0.00814	0.00660
σ^* S_1-C_7	−0.01780	−0.01616	−0.01678	−0.03329	−0.03500
σ^* C_7-H_8	0.00189				−0.00830
σ^* C_7-H_9		0.00475	0.00378	0.00497	0.00415
σ^* C_7-H_{10}			0.00256		0.00172
σ^* $O_{11}-H_{12}$	0.04557				
σ^* $O_{11}-H_{13}$	0.00149	0.03352	0.00418	0.03108	0.00247
σ^* $O_{14}-H_{15}$				0.03271	0.00720
σ^* $O_{14}-H_{16}$			0.03647		0.03389
σ^* $O_{17}-H_{18}$					0.03527
σ^* O_17-H_{19}					

The NBO analysis (Table 6) shows a large ED decrease in the σ^* antibonding orbitals of both S−C bonds. This effect leads to a contraction of both S−C bonds. A significant ED decrease is also evident in the σ^* antibonding orbital of the C_7-H_8 bond, which should lead to bond contraction. The respective ED change is significant (−0.0083e). Other changes of ED in the remaining C−H antibonding orbitals are, however, positive and cannot be thus used for the interpretation of changes of respective C−H stretch vibrational frequencies (cf. Table 3). Therefore, an additional mechanism should be reconsidered.

The large CT between DMSO and three water molecules also causes, besides discussed changes in the ED of bonding and antibonding orbitals, changes in the electronic state of DMSO. This is mainly reflected by the changes of atomic ED resulting in changes in hybridization. This is not an entirely new effect, and we described it recently[35] when discussing the blue shift of the amino N−H stretch vibrational frequency of guanine upon the formation of the guanine dimer. It was shown[35] that this shift was due to a planarization of the guanine amino group caused by a decrease of ED at the amino group nitrogen, which resulted in a change of nitrogen hybridization. The NBO analysis performed for the DMSO···$(H_2O)_3$ complex tells us that the s character of sp^n hybrid orbitals for the C_3-H_5 and C_7-H_{10} bonds of DMSO increases upon the formation of a complex (from $sp^{2.82}$ to $sp^{2.74}$ for C_3-H_5 and from $sp^{2.89}$ to $sp^{2.79}$ for C_7-H_9). An increase of s character results in the strengthening of a bond. Because the former effect (i.e., increase of ED in σ^* antibonding orbitals) is not pronounced for these bonds, we can expect that they will become shorter upon complex formation. By investigating Tables 3 and 6, we found that this really happened.

We can conclude our discussion of the NBO analysis by saying that there are two ways to decrease the C−H bond length and obtain a blue shift of the stretch vibrational frequency. The first—a direct way—is connected with a decrease of ED in the σ^* antibonding orbital, which yields bond contraction and a blue shift of this stretch frequency. The second way is connected with the rehybridization of sp^n C−H hybrid orbitals. A change of electronic state caused by CT within a complex brings an increase in the s character of the hybrid bond, which is

manifested by bond contraction and a blue shift of the C−H stretch frequency.

Both mechanisms presented above are due to changes of ED in DMSO upon hydration. There also exist, however, other mechanisms to explain the contraction of C−H bonds in DMSO upon complex formation. The first is connected with the dominant geometry change occurring as a result of complex formation (i.e., the elongation of the S═O bond).

This effect will be now investigated in more detail; the respective calculations were performed at the MP2/6-31G** level. First, we fully optimized the isolated DMSO. In the second step, we again optimized the isolated DMSO but now with an elongated S═O bond taken from the optimized DMSO···$(H_2O)_3$ complex, and this bond was kept frozen during the optimization. Comparing the bond lengths, we found that both S−C bonds were contracted (by 0.0021 and 0.0024 Å for the S_1-C_3 and S_1-C_7 bonds, respectively) and also that four of the six C−H bond were contracted. The largest contraction was found for the C_3-H_4 and C_7-H_8 bonds (0.00022 Å). It is thus evident that the elongation of the S═O bond affects the geometrical structure. The C−H and the S−C contractions induced in the isolated DMSO by the elongation of S═O bond are, however, smaller than those in the DMSO···$(H_2O)_3$ complex, which supports the fact that another effect participates. In the following discussion, the role of the electrostatic field of hydrating waters will be briefly investigated.

DMSO was optimized in the electrostatic field generated by the point charges of three water molecules in the geometry taken from the DMSO···$(H_2O)_3$ complex. The applied field leads to the elongation of the S═O bond by 0.0142 Å and to the contraction of the C_3-H_5 and $S-C_3$ bonds by 0.00025 and 0.01147 Å, respectively. The changes of the first two coordinates are about 3 and 7 times smaller than those in the complex, and only the change of the last one agrees. In this case, the optimization was performed with respect to the coordinates that were mentioned. In the second step, the whole geometry was optimized, and the geometry changes that were found are much closer to these obtained by the quantum chemical optimization. The only exception concerns the S═O bond, which in the applied electrostatic field is contracted and not elongated. It is thus evident that isolated electrostatic effects themselves cannot explain the geometry (and vibration) changes of DMSO upon hydration, and evidently, only the concerted action of all three effects (geometry changes induced by EDT, effects of EDT, and electrostatic effects) can explain them. Not one of these three effects by itself can interpret the experimental (and also theoretical) finding of the C−H blue shift increase upon progressive hydration.

DMSO−Continuous Solvent. COSMO calculations were performed at the DFT/6-31G** level. First, the isolated DMSO was optimized at this level, and in the second step, the DMSO in a continuous solvent was investigated. We found that only S−C bonds were contracted (by ∼0.010 Å) whereas all other bonds were elongated. Vibrational analysis revealed that the S═O stretch was red-shifted by about 25 cm^{-1}, and smaller red shifts were observed for all C−H stretches (1−5 cm^{-1}). Thus, it is evident that the continuous solvent model cannot correctly predict the changes of geometry and vibrational stretching modes of DMSO upon hydration, which are clearly very specific and directed.

IV.3. Mechanism of the Hydration of DMSO and Comparison with the Experiment. Combining the results from quantum chemical calculations and MD simulations, we can interpret the experimental data on progressive hydration as follows. The first few molecules hydrate the sulfo group, and at this stage, the elongation of the bond plays a decisive role in explaining the contraction (and blue shifts) of the C−H bonds. Within a few waters, the S═O group is, however, saturated, and other waters start to hydrate the methyl groups, and the S═O bond length is changed only slightly (see Tables 3−5). The further growth of the C−H bond contraction and the blue shift of the C−H stretch vibrations is realized mainly through changes of ED in the σ^* antibonding orbitals and changes of hybridization of the C−H hybrid bonds. An increasing electrostatic field of hydrating waters plays also an important role.

Vibrational analysis performed at the RI-MP2/TZVPP level for the largest cluster (DMSO···$(H_2O)_3$) yields the following results on the average blue shift of the CH stretch vibrations and the red shift of the S═O stretch vibration: 10 and 77 cm^{-1}. The respective experimental data[5] are 17 cm^{-1} for the C−H blue shift and 50 cm^{-1} for the S═O red shift. Taking into account the above cited mechanism of the DMSO hydration, we must expect a further increase of the theoretical C−H blue shift upon increasing the hydration number. However, the theoretical value of the S═O red shift is close to saturation. In light of these extrapolations, the agreement between RI-MP2/TZVPP calculations (no scaling was used) and experiment should be considered satisfactory.

V. Conclusions

(1) MD simulations give evidence of the preferential hydration sites of DMSO. First, waters hydrate the S═O group, and by adding more waters, the full hydration shell was formed where the S═O as well as the methyl groups were hydrated.

(2) The interaction of water molecules with the S═O group leads to the formation of a standard H-bond characteristic by the elongation of the S═O bond and the red shift of the stretching vibration. The elongation of the S═O bond triggered the geometry changes in the DMSO subunit leading to a contraction of the C−H bonds with the concomitant blue shifts of the respective stretch frequencies. The mechanism described is not unusual, and a very similar one was found in our recent experimental and theoretical study on $(CH_3)_2O\cdots HCF_3$.[22] The EDT from oxygen-induced geometry reorganization in the $(CH_3)_2O$ subunit was followed by a contraction of the C−H bonds and concomitant blue shifts of the C−H stretches. Theoretical and experimental values of the blue shift agreed quite well.[22] Besides the geometrical factor, the changes of ED within DMSO upon hydration also play a role. It concerns the direct decrease of ED in the σ^* antibonding orbitals of C−H bonds as well as the rehybridization of sp^n bonds leading (both) to a contraction of the respective C−H bonds and a concomitant blue shift of the C−H stretch vibrational frequency. When water interacts directly with the methyl groups of DMSO, a contraction of the C−H bonds is mainly due to the electrostatic field of hydrating water molecules.

(3) The red shift of the S═O bond is saturated by the addition of only three waters; the largest increase of the shift is found when the second water is added. However, the blue shift of the C−H stretches increases linearly with the increased hydration number.

(4) The linear enhancement of the blue shifts of the C−H stretches upon progressive hydration that is found experimentally can be explained only if all of the effects (elongation of the S═O bond, changes of ED in DMSO, and the electrostatic field of waters) are considered simultaneously.

(5) The proposed mechanism of the C−H blue shift is identical to that found in many other improper blue-shifting H

bonds (amino N−H···O in the guanine dimer,[35] C−H···O in $(CH_3)_2$···HCF_3,[22] C−H··· in CH_4···C_6H_6 and CCl_3H···C_6H_6,[10] C−H··· in CCl_3H···C_6H_5F,[12,13] C−H···O in CF_3H···$O(CH_2)_2$,[14] C−H···O in CX_3H···OH_2 (X = F, Cl, Br),[23] X^-···H_3CY (X = Cl, I; Y = Br, I),[11,16] and N−H···F in NF_2H···FH[36]). In the present system as well as in the above-mentioned complexes, the changes of ED were smaller than in standard H-bonded systems and did not occur in the adjacent parts of interacting molecules but in their remore parts. Worth mentioning is the fact that theoretical findings (in the present papers as well as in mentioned studies[11,13,16,22,35]) were consistent with experimental results. Furthermore, the mechanism suggested in the present study is in our opinion more justified than the "pushball" hydration model suggested in ref 5. A simple argument against the main feature of the "pushball" model (the electrons of the C−H hydrogen are pushed toward the carbon atom because of a dispersion interaction with the electrons of water oxygen; cf. ref 5) is based on the fact that reliable theoretical data on the presented complexes were obtained not only at the RI-MP2 and MP2 levels but also at the Hartree−Fock level, which completely neglects the dispersion interaction.

Acknowledgment. This project, LN00A032 (Center for Complex Molecular Systems and Biomolecules), has been supported by the Ministry of Education of the Czech Republic.

References and Notes

(1) Carius, W.; Mockel, K.; Schroter, O.; Thomzik, D. *Z. Phys. Chem. (Leipzig)* **1982**, *263*, 209.
(2) Tomzik D.; Schroter, O.; Walter, I.; Mockel, K. *Z. Phys. Chem. (Leipzig)* **1990**, *271*, 347.
(3) Kamogawa, K.; Kitagawa, T. *J. Phys. Chem.* **1986**, *90*, 1077.
(4) Pohle, W.; Gauger, D. R.; Fritzsche, H.; Rattay, B.; Selle, C.; Binder, H.; Böhlig, H. *J. Mol. Struct.* **2001**, *463*, 563
(5) Mizuno, K.; Imafuji, S.; Ochi, T.; Ohta, T.; Meada, S. *J. Phys. Chem. B* **2000**, *104*, 11001.
(6) Scheiner, S. *Hydrogen Bonding: A Theoretical Perspective*; Oxford University Press: Oxford, U.K., 1997.
(7) Trudeau, G. T.; Dumas, J. M.; Dupuis, P.; Guerin, M.; Sandorfy, C. *Top. Curr. Chem.* **1980**, *93*, 91.
(8) Budešinský, M.; Fiedler, P.; Arnold, Z. *Synthesis* **1989**, 858.
(9) Boldeskul, I. E.; Tsymbal, I. F.; Ryltsev, E. V.; Latajka, Z.; Barnes, A. J. *J. Mol. Struct.* **1997**, *167*, 436.
(10) Hobza, P.; Špirko, V.; Sezle, H. L.; Schlag, E. W. *J. Phys. Chem. A* **1998**, *102*, 2501.
(11) Hobza, P.; Havlas, Z. *Chem. Rev.* **2000**, *100*, 4253.
(12) Hobza, P.; Špirko, V.; Havlas, Z.; Buchhold, K.; Reimann, B.; Barth, H. D.; Brutschy, B. *Phys. Chem. Lett.* **1999**, *299*, 180.
(13) Reimann, B.; Buchhold, K.; Vaupel, S.; Brutschy, B.; Hobza, P.; Havlas, Z. *J. Phys. Chem. A* **2001**, *105*, 5560.
(14) Hobza, P.; Havlas, Z. *Chem. Phys. Lett.* **1999**, *303*, 447.
(15) Gu, Y.; Scheiner, S. *J. Am. Chem. Soc.* **1999**, *121*, 9411.
(16) Hobza, P.; Havlas, Z.; Johnsson, M. Unpublished results, 2001.
(17) Karger, A.; Amorim da Costa, A. M.; Ribeiro-Claro, P. J. A. *J. Phys. Chem. A* **1999**, *103*, 8672.
(18) Caminati, W.; Melandri, S.; Moreschini, P.; Favero, P. G. *Angew. Chem., Int. Ed.* **1999**, *38*, 2924.
(19) Mizuno, K.; Imafuji, S.; Ochi, T.; Ohta, T.; Maeda, S. *J. Phys. Chem. B* **2000**, *104*, 11001.
(20) Masunov, A.; Dannenberg, J. J.; Contreras, R. H. *J. Phys. Chem. A* **2001**, *105*, 4737.
(21) Hartmann, M.; Wetmore, S. D.; Radom, L. *J. Phys. Chem. A* **2001**, *105*, 4470.
(22) Van der Vaken, B. J.; Herrebout, W. A.; Szostak, R.; Shchepkin, D. N.; Havlas, Z.; Hobza, P. *J. Am. Chem. Soc.* **2001**, *123*, 12290.
(23) Zierkiewicz, W.; Michalska, D.; Havlas, Z.; Hobza, P. *ChemPhysChem* **2002**, *3*, 511.
(24) Ford, T. A.; Glasser, L. J. *J. Mol. Struct.: THEOCHEM* **1997**, *381*, 398.
(25) Alkorta, I.; Rozas, I.; Elguero, J. *Int. J. Quantum Chem.* **2002**, *86*, 122.
(26) Reed, A. E.; Curtiss, L. A.; Weinhold, F. *Chem. Rev.* **1988**, *88*, 899.
(27) Vishnyakov, A.; Lyubartsev, A. P.; Laaksonen, A. *J. Phys. Chem. A* **2001**, *105*, 1702.
(28) Hermansson, K. *J. Phys. Chem. A* **2002**, *106*, 4695.
(29) Trygubenko, S. A.; Bogdan, T. V.; Rueda, M.; Orozco, M.; Lugue, F. J.; Šponer, J.; Slavíček; Hobza, P. *Phys. Chem. Chem. Phys.* **2002**, *4*, 4192.
(30) Hobza, P.; Riehn, Ch.; Weichert, A.; Brutschy, B. *Chem. Phys.* **2002**, *283*, 321.
(31) Boys, S. F.; Bernardi, F. *Mol. Phys.* **1970**, *19*, 553.
(32) Ahlirchs, R.; Bär, M.; Häser, M.; Horn, H.; Kölmel, C. *Chem. Phys. Lett.* **1989**, *162*, 165.
(33) Frisch, M. J.; Trucks, G. W.; Schlegel, H. B.; Scuseria, G. E.; Robb, M. A.; Cheeseman, J. R.; Zakrzewski, V. G.; Montgomery, J. A., Jr.; Stratmann, R. E.; Burant, J. C.; Dapprich, S.; Millam, J. M.; Daniels, A. D.; Kudin, K. N.; Strain, M. C.; Farkas, O.; Tomasi, J.; Barone, V.; Cossi, M.; Cammi, R.; Mennucci, B.; Pomelli, C.; Adamo, C.; Clifford, S.; Ochterski, J.; Petersson, G. A.; Ayala, P. Y.; Cui, Q.; Morokuma, K.; Malick, D. K.; Rabuck, A. D.; Raghavachari, K.; Foresman, J. B.; Cioslowski, J.; Ortiz, J. V.; Stefanov, B. B.; Liu, G.; Liashenko, A.; Piskorz, P.; Komaromi, I.; Gomperts, R.; Martin, R. L.; Fox, D. J.; Keith, T.; Al-Laham, M. A.; Peng, C. Y.; Nanayakkara, A.; Gonzalez, C.; Challacombe, M.; Gill, P. M. W.; Johnson, B. G.; Chen, W.; Wong, M. W.; Andres, J. L.; Head-Gordon, M.; Replogle, E. S.; Pople, J. A. *Gaussian 98*, revision A.7; Gaussian, Inc.: Pittsburgh, PA, 1998.
(34) Barone, V.; Cossi, M.; Tomasi, J. *J. Comput. Chem.* **1998**, *19*, 404.
(35) Hobza, P.; Špirko, V. *Phys. Chem. Chem. Phys.*, submitted for publication.
(36) Hobza, P. *Int. J. Quantum Chem.* **2002**, *90*, 1071.